Characterization and Probabilistic Modeling of the Mesostructure of Parallel Strand Lumber

Alireza Amini[1]; Sanjay R. Arwade[2]; Peggi L. Clouston, A.M.ASCE[3]; and Saranthip Rattanaserikiat, S.M.ASCE[4]

Abstract: Parallel strand lumber (PSL) is a composite made of oriented wood strands that have been glued and compressed together. Its market share in the residential construction industry is considerable, being used primarily as main load bearing members such as beams and columns. Unlike the fast-paced market growth of these products, computational development has been slow. The highly heterogeneous mesostructure of this material must be known and quantified in order to develop advanced computational tools for limit state analysis of PSL. Void heterogeneities play an important role in determining the failure modes and strength of PSL, in addition to material phase aberrations such as grain angle variations and defects. In this study, two-dimensional (2D) and three-dimensional (3D) void characteristics were investigated. An experimental program along with a statistical survey was conducted to quantify the following 2D and 3D void characteristics in two $133 \times 133 \times 610$ mm PSL billets: volume fraction, volume, alignment, and moments of inertia of voids, as well as second moment properties, lineal path function, and chord length functions of the two phase mesostructure. As expected, most of the voids lie on the longitudinal direction of the specimen and have approximately an ellipsoidal shape. Based on this shape data, the characteristics of the ellipsoids that best fit the voids were calculated. Using the statistical data of the fitted ellipsoids, a random field of virtual ellipsoidal voids to simulate the mesostructure of PSL was generated. **DOI: 10.1061/(ASCE)MT.1943-5533.0001116.**

Author keywords: Parallel strand lumber; Wood composite; Mesostructure; Void characterization; Probabilistic modeling.

Introduction

Since its inception, parallel strand lumber (PSL) has become increasingly popular in light-frame construction as a reliable supplement and replacement for traditional solid-sawn lumber (SSL). PSL is produced by just one manufacturer, Weyerhaueser, under a patent-protected process. It is composed of thin strands of oriented wood veneer compacted and glued together with phenol-resorcinol and phenol-formaldehyde based adhesive (Fig. 1). Reduction and dispersion of wood knots and defects in the process of manufacturing result in lower material property variability compared to that of SSL (U.S. Forest Products Laboratory 2010; Mindess et al. 2004). Another important advantage is that the desired length and width of PSL can be economically produced regardless of the size of the trees available. Also, because many species can be used almost interchangeably, more timber harvested from a single stand can be utilized.

In spite of the significant increase in the production and demand of PSL, the development of computational tools for the analysis and design of PSL members has advanced very slowly. Research is necessary to develop accurate constitutive models and computational tools for predicting the strength of the material. To this end, a comprehensive statistical characterization of the mesostructure (which is defined as consisting of wood strands, adhesive and the voids remaining after compaction) is needed.

This study focuses on the characterization of PSL voids as one of the main features of this material's mesostructure. Voids affect most, if not all, of the mechanical properties of PSL members, specifically the elastic constants, yield stress, and ultimate stresses in tension and compression. Some of these properties, such as elastic modulus, are primarily sensitive to the overall void fraction, while others such as yield and ultimate stress are also highly sensitive to the shape, orientation, and spatial distribution of the voids. The degree of sensitivity of various mechanical properties to the void structure has been investigated and reported in Amini (2013) and Amini et al. (2013). The objective of this study is to quantify the statistics of shape, orientation, and location of the voids in PSL material and to find a probabilistic model that represents actual void statistics. To clarify the difference between mesostructure and microstructure of PSL (the latter is not included in this work), PSL's microstructure is the same as that of the species used to manufacture PSL. The PSL specimens studied in this work are made of Eastern species (especially southern pine) that are classified as softwood. The microstructure of softwood consists predominantly of long, thin walled, 3–5-mm-long tubular cells called tracheids that have a diameter ranging from 20 to 80 μm. The longitudinal tracheids constitute about 90% volume of the softwood and serve both the conductive and mechanical needs of the organic material. The large open space in the center of the cell is called the lumen, which is used for water conduction (U.S. Forest Products Laboratory 2010). The diameter of voids investigated in this work is at least one order of magnitude larger than that of tracheids.

Only three previous studies were found to have worked on geometry characterization of PSL. Elis et al. (1994) studied the macroporosity of PSL by two optical techniques. They used a video camera and a line scan camera to capture the voids of PSL in

[1]Research Fellow, Dept. of Civil and Environmental Engineering, UMass Amherst, 130 Natural Resources Rd., Amherst, MA 01003 (corresponding author). E-mail: aamini@engin.umass.edu

[2]Associate Professor, Dept. of Civil and Environmental Engineering, UMass Amherst, 130 Natural Resources Rd., Amherst, MA 01003.

[3]Associate Professor, Dept. of Environmental Conservation, UMass Amherst, 160 Holdsworth Way, Amherst, MA 01003.

[4]Graduate Student, Dept. of Civil and Environmental Engineering, Johns Hopkins Univ., Latrobe Hall 205, 3400 North Charles St., Baltimore, MD 21218.

Note. This manuscript was submitted on August 29, 2013; approved on April 28, 2014; published online on August 12, 2014. Discussion period open until January 12, 2015; separate discussions must be submitted for individual papers. This paper is part of the ***Journal of Materials in Civil Engineering***, © ASCE, ISSN 0899-1561/04014179(10)/$25.00.

transmitted light and then analyzed the images. In another work, Sugimori and Lam (1999) used X-ray computer tomography techniques on a $0.16 \times 0.34 \times 1.28$ m PSL specimen and made a database of distribution of size and position of macro voids in three-dimensional (3D) space. And in Clouston (2007), macroporosity was defined along the transverse-longitudinal plane through enhanced image analyses. A histogram of percentage void content in the longitudinal-transverse plane of PSL was presented, but no work was done to define specifically the void size, shape and location, as is the focus of this work.

Compared to the mesostructural characterization, more studies have been done on the constitutive modeling of PSL and similar materials. In 2001, a nonlinear stochastic model was formulated by Clouston and Lam (2001) to simulate the stress-strain behavior of a PSL-like product, but without voids and based on the constitutive properties of the wood strands only. The model, characterized within the framework of rate-independent orthotropic plasticity using Tsai-Wu failure theory, was a novel approach and was successful in predicting the experimental behavior of several wood angle-ply laminate configurations. Later, Clouston (2007) expanded on this work to incorporate measured macroporosity and grain angle variation of PSL to model the mechanical properties of small coupons of PSL. Excellent results were found when the computed and experimental data sets were compared, validating the modeling technique. In 2004, Bejo and Lang (2004) proposed a different probability based model to study the effect of the change in elastic properties only, on the performance of structural composite lumber products. They also modeled the orthotropic behavior of wood constituents due to their position in the composite by theoretical/empirical equations. Also focused on spatial variation of the elastic modulus of PSL, Arwade et al. (2009) proposed a stochastic computational model that incorporates orthotropic elasticity and uncertainty in strand geometry and material properties. They found good agreement between their model and bending test results. The same authors investigated the variability of compressive strength of PSL by conducting the measurement of compressive strength on specimens of varying size with nominal identical mesostructure (Arwade et al. 2010). They also developed a computational model including the strand length, grain angle, elastic constants and parameters of a Tsai-Hill failure surface.

In this study, the focus is on statistically characterizing the void structure of PSL and incorporating it into a probabilistic mechanical model. The mesostructure of PSL has been measured using a serial sectioning technique followed by a computational approach to relate the measurements in each section. There could be variation in the void structure of PSL members made at different plants or with different species mixes. Such variation has not been investigated in this paper, yet the experience of the authors indicates that the qualitative features of the void model presented here would not need to be modified in order to model the void structure of other batches of PSL. Therefore, the modeling of the void structure in other batches is reduced to a model calibration problem that is not fundamentally dissimilar from that used to calibrate any material model such as an elastic-plastic constitutive model. The question of applicability of the model across batches is certainly a question worthy of further investigation. Regarding the question of variability across member size, the authors' understanding is that PSL is manufactured in large billets of uniform size and then sawn to the reduced sections commonly available for retail and wholesale purchase. Therefore, there is little reason to expect that there would be differences in void structure across member sizes.

Experimental Approach to Characterize Void Structure

All specimens used for the mesostructural characterization studies were machined from 2.0E Eastern Species PSL billets manufactured by iLevel by Weyerhaeuser. All specimens were conditioned to ambient laboratory conditions for one month before testing and reached an equilibrium moisture content of 8–11%.

Orthotropic in a global sense, the physical and mechanical variability in strands along with the voids result in material heterogeneity and geometric randomness. The applied coordinate system has been shown in Fig. 1 in which L, T, and TT axes represent longitudinal, transverse, and thru thickness directions of PSL,

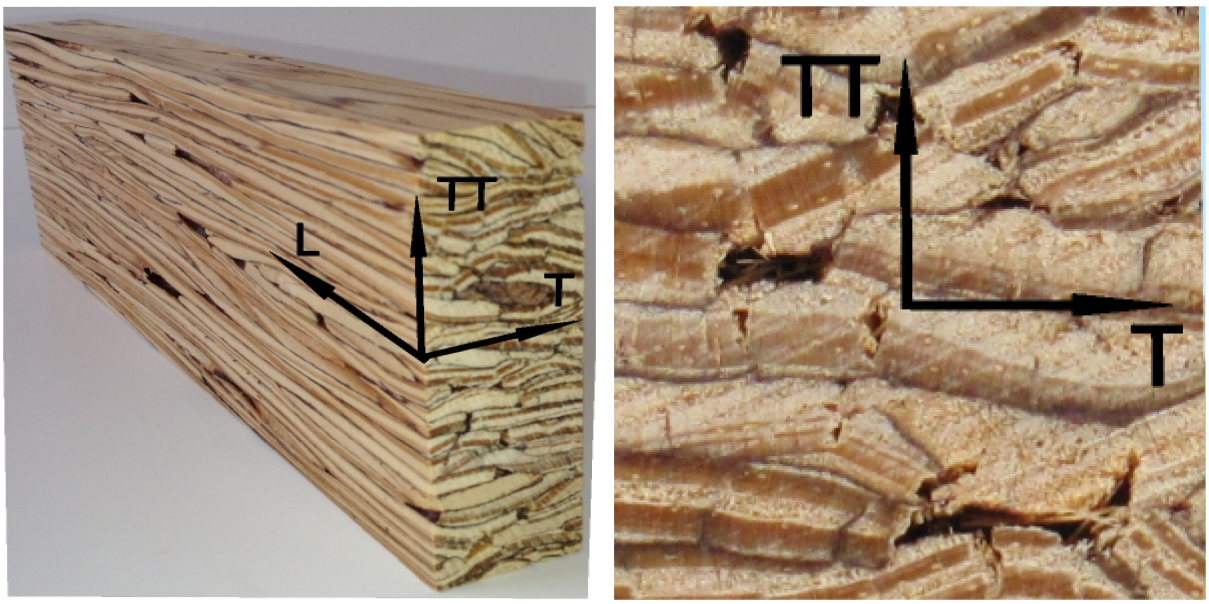

Fig. 1. Cross-sectional views of PSL specimen and definition of the member coordinate system; L = longitudinal, T = transverse, TT = thru thickness: (a) 3D view; (b) T-TT section

respectively. Beginning with two $133 \times 133 \times 610$ mm billets of PSL (both cut from the same bigger billet) a serial sectioning and scanning approach was used to reconstruct the three-dimensional void structure of the billet.

Void Measurement Procedure

T-TT sections were cut using a band saw with a 6 teeth per inch blade. These sections were then painted white to provide high contrast between the void phase and the solid wood phase. Painting the sections in this way eased identification of the void phases but obscured information regarding the strand geometry. Here only the results regarding the void phase are presented. Each section of the T-TT plane was scanned to a grayscale image at 100 pixels per inch. These scans were then digitally stacked in the L direction to reconstruct the full three-dimensional void structure of the billet. It was observed that the sections absorbed a small amount of moisture during the painting process, slightly expanding the sample in the T and TT directions by 0.8% in the T direction and 2% in the TT direction. The thickness of each section was measured at the time of cutting, and the sum of the section thicknesses was compared to the original longitudinal length of the specimens to establish the average saw kerf thickness. The average section thickness was found to be 2.75 mm and the average saw kerf thickness was found to be 1.30 mm. Given these measurements, each voxel in the three-dimensional mesostructure reconstruction has physical dimensions (T-TT-L) of $0.252 \times 0.248 \times 4.02$ mm.

The process of digitally stacking the scans and void detection was time consuming. Each void voxel was checked to see if it neighbored any other void voxel, and if so, the neighboring void voxels were considered parts of a long (i.e., more than a voxel long) void. More than 17,000 voids were found in the first billet, while the number of voids in the second billet exceeded 20,000. Among these voids, 43% of the voids in the first billet and 49% in the second billet were just a single voxel in each direction. Therefore, there are many tiny voids in a PSL specimen, but on the other hand, there are also considerably large voids that theoretically can influence the mechanical behavior of material. The largest void in the first and second billets have respectively about 44,000 and 72,000 voxels. In other words, their volumes are about 11,000 and 18,000 mm^3, respectively. The codes written in *MATLAB* facilitated this data-processing procedure.

Two-Dimensional Statistical Characterization of the Void Structure

A distinctly anisotropic nature of the void structure is clearly visible in Fig. 2. In the T-TT view, voids look rather isotropic and uniformly dispersed; on the contrary, in the L-T and L-TT views, voids are obviously elongated in the L direction. The strands are also elongated mainly in L direction; hence, the voids tend to spread correlated to the strand dimension. This correlation is also tangible along T and TT directions. Because the wider dimension of the strands is predominantly oriented in T direction, the voids in L-T view apparently have a larger size in the T direction than do the voids in L-TT view in TT direction. In other words, the aspect ratio of voids' axes lengths in T-TT view (i.e., the length of void along T axis over the length of void along TT axis) is not one, but more (Table 1). The simplest characterization of the mesostructure is the volume fraction of the void phase, which for the first and second billets was respectively found to be 2.4 and 2.8%. More complete

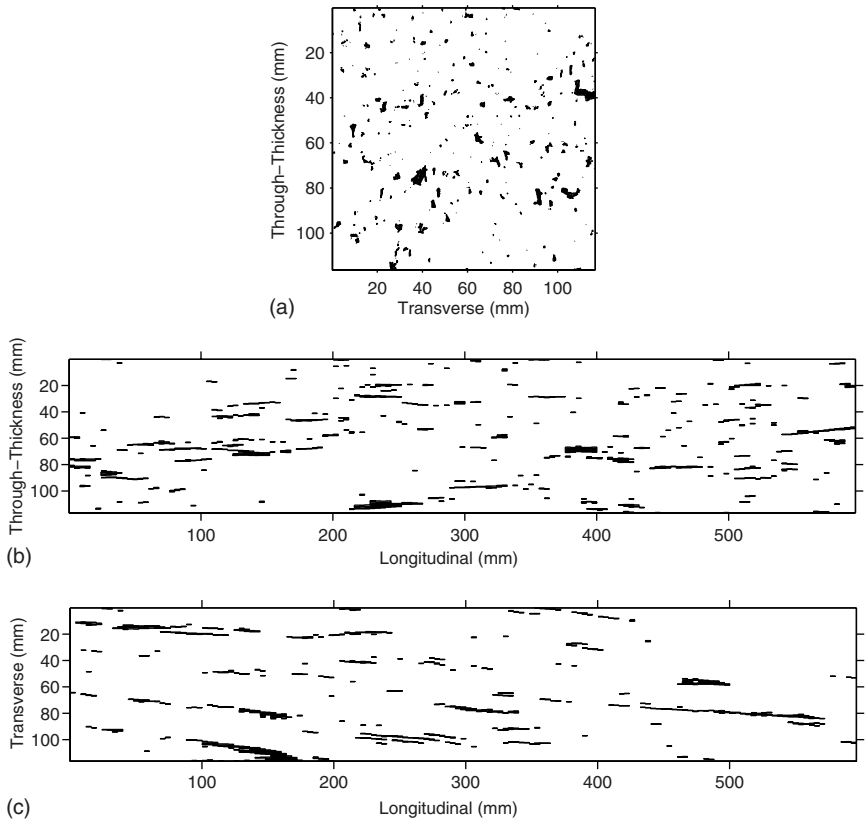

Fig. 2. Three section views through the three-dimensional reconstruction of the PSL mesostructure; black regions represent void and white regions represent wood strands: (a) T-TT section; (b) L-TT section; (c) L-T section

Table 1. Statistics of the Void Properties for Three Orthogonal Sections Obtained from 2D Investigation

Property	Statistical measure	First billet			Second billet		
		T-TT	L-T	L-TT	T-TT	L-T	L-TT
Major axis length	Mean (mm)	1.2	9.1	9.6	1.1	9.6	10.2
	Median (mm)	0.6	4.6	4.6	0.6	4.6	4.6
	Standard deviation (mm)	1.4	10.9	11.4	1.4	12.1	12.6
Minor axis length	Mean (mm)	0.6	0.8	0.8	0.6	0.8	0.7
	Median (mm)	0.3	0.6	0.6	0.3	0.4	0.4
	Standard deviation (mm)	0.6	1.0	0.8	0.6	1.0	0.8
Aspect ratio	Mean	1.8	13.5	13.9	1.7	14.8	15.4
	Median	1.6	16.0	16.0	1.5	16.0	16.0
	Standard deviation	0.9	6.4	6.3	0.9	6.6	7.1
Area	Mean (mm^2)	0.87	8.22	7.73	0.78	8.96	7.72
	Median (mm^2)	0.19	2.00	2.00	0.13	2.00	2.00
	Standard deviation (mm^2)	2.28	25.35	21.99	2.23	28.91	22.79

characterizations of the mesostructure would include the voids size distribution and some measure of the void shape. Below, characterizations of two dimensional cross sections of the mesostructure, such as those shown in Fig. 2, are presented.

The basic statistics obtained from the two-dimensional (2D) investigation has been presented in Table 1. The data show that in both billets, the length aspect ratio in T-TT sections is about 2, while it is about 25 in L-T and L-TT sections. These values match what is observed in Fig. 2.

The two-point probability function provides a first order characterization of the spatial arrangement of the phases of a heterogeneous material (Torquato 2002). Considering the heterogeneous material to occupy a domain Ω and to consist of two phases that occupy Ω_1 and Ω_2 such that $\Omega_1 \cup \Omega_2 = \Omega$ and $\Omega_1 \cap \Omega_2 = \phi$. The coordinate axes will be called a_1 and a_2 in the 2D space. The two-point probability function is defined to be

$$S_1(d,\theta) = Pr(x_1 \in \Omega_1 \cap x_2 \in \Omega_1) \tag{1}$$

the probability that both points x_1 and x_2 are in Phase 1. In the case where the heterogeneous material is stationary and statistically isotropic, the two-point probability function depends only on $d = ||x_1 - x_2||$. If, on the other hand, the material is stationary but statistically anisotropic the two-point probability function can be defined as a function of $d = ||x_1 - x_2||$ and $\theta = \text{atan}\{[(x_2)_2 - (x_1)_2]/[(x_2)_1 - (x_1)_1]\}$ the distance of separation between the two points and the angle between a line connecting the two points and the a_1 axis [$(x_i)_j$ is the jth component of the position vector x_i]. When $x_1 = x_2$ the value of this function is simply the volume fraction of Phase 1. And when x_1 and x_2 are widely separated, their probabilities of occurrence do not affect each other (i.e., the points are uncorrelated and statistically independent), therefore the value of function approaches the product of probabilities that either points are in Phase 1, which equals the square of Phase 1 volume fraction. The authors have estimated the two-point probability functions in the T-TT, L-T, and L-TT planes of the first billet, treating Phase 1 as the void phase (Fig. 3), which clearly show the anisotropy present in the L-T and L-TT planes. The T, L, and L directions correspond to $\theta = 0$ in the three figures showing that the voids are elongated in the L direction, and perhaps very slightly in the T direction for the T-TT plane. A mild anisotropy in the T-TT plane is supported by the deviation of the mean aspect ratio from unity in the T-TT plane. One can observe that the decay lengths of the two-point probability functions correspond to the average dimensions of the voids in the various material directions on the various planes.

Another useful statistical measure for void 2D characterization is the lineal path function. For statistically isotropic media, lineal path function is defined as probability that a line segment of length d lies wholly in void phase when randomly thrown into the sample (Torquato 2002). Consider a heterogeneous material consisting of two phases that occupy Ω_1 and Ω_2. The line $\overline{x_1 x_2}$ with the length $d = ||x_1 - x_2||$ and angle $\theta = \text{atan}(([x_2]_2 - [x_1]_2)/([x_2]_1 - [x_1]_1))$ with the a_1 axis connects two random points x_1 and x_2 in the material. The lineal path function $L_1(d)$ is defined by Eq. (2)

$$L_1(d,\theta) = Pr(\overline{x_1 x_2} \in \Omega_1) \tag{2}$$

When the line's length (d) is zero, the lineal path function is equal to the void volume fraction; and when d is infinite, the lineal

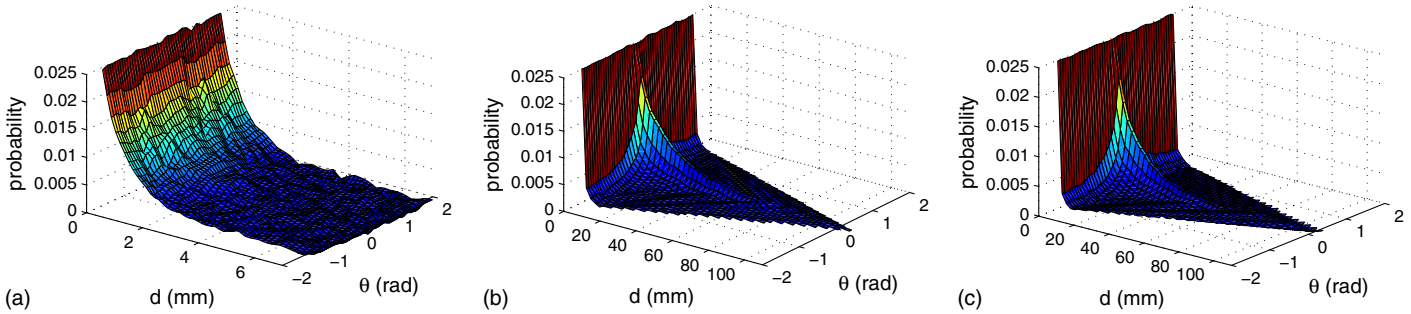

Fig. 3. Two-point probability functions for the first PSL billet: (a) T-TT section; (b) L-TT section; (c) L-T section

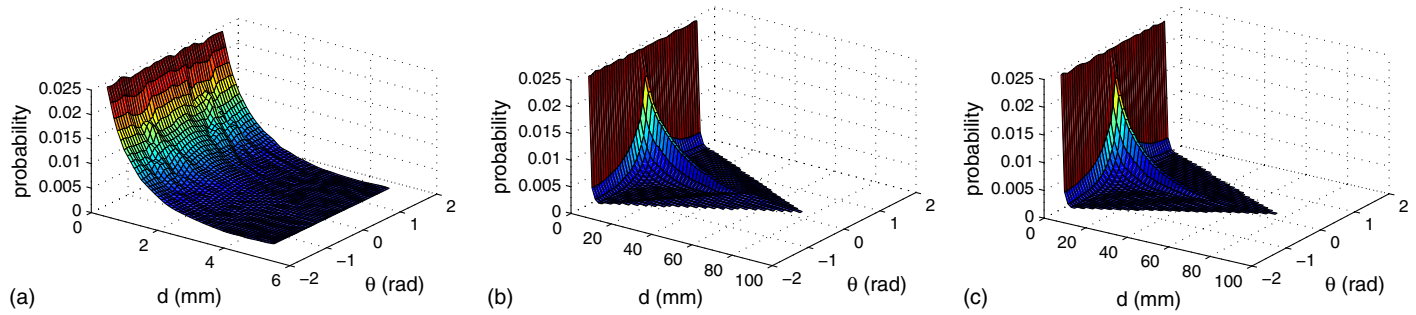

Fig. 4. Lineal path functions for the first PSL billet: (a) T-TT section; (b) L-TT section; (c) L-T section

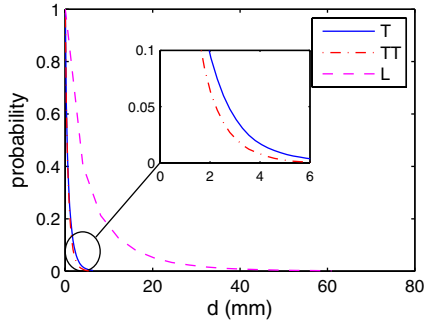

Fig. 5. Chord length density function in all three material directions of the first PSL billet

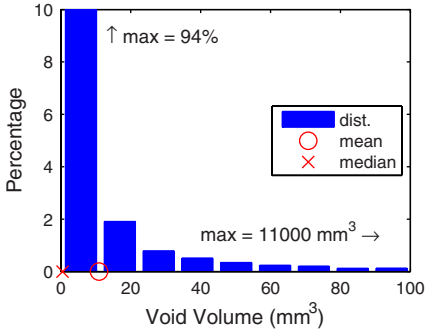

Fig. 6. Distribution of volume of the first PSL billet voids

path function equals zero. Fig. 4 illustrates the lineal path function evaluated in the T-TT, L-T, and L-TT planes of the first billet. The results are quite similar to the two-point probability function. One can infer from this similarity that the voids in PSL do not have wry and crooked shapes; therefore, when two points are in the void phase, the line connecting them is most probably in the same phase.

The last measure to obtain the 2D characteristics of voids is the chord length density function, which is defined as the probability of finding a chord of length between d and $d + \Delta d$ in void phase (Torquato 2002). This measure is useful for the estimation of average void length. Consider a chord $\overline{AB}$ with the length $|\overline{AB}|$ lying fully in the void phase ($\overline{AB} \in \Omega_1$). The chord length density function is defined as

$$p_1(d, \theta) = Pr(d \leq |\overline{AB}| \leq d + \Delta d) \tag{3}$$

Based on the definition, when the chord length is zero, the chord length density function is equal to 1, and when the length is infinite, the function equals zero. To simplify the calculations, only the chord length function for the directions parallel to coordinate axes was estimated. Fig. 5 displays the chord length density functions in the TT, T, and L directions for the first billet. The results clearly show that the longitudinal direction contains larger void lengths and that the voids in the L-T and L-TT sections are elongated, with approximate average aspect ratio of 10, in L direction.

Because (1) the number of figures related to the statistics of void shapes in each billet is large, and (2) the investigation showed that the shapes of voids in these two billets have similar statistical properties, it is efficient not to double the number of figures and to display merely the statistics of the void shapes in the first billet. This choice has also been kept in the other sections throughout this paper. The tables, nevertheless, contain the data of both billets.

Three-dimensional Statistical Characterization of the Voids Structure

Direct Characterization

The voids occupy 2.4 and 2.8% of the volume of first and second billets. In both billets, the mean value of individual void's volume is 11 mm^3, but its median is much less (0.5 mm^3 that equals the volume of two voxels). Therefore, the void volume distribution is highly skewed. Fig. 6 along with the calculated values of skewness (40 in the first and 60 in the second billet), kurtosis (2,250 in the first and 5,100 in the second billet) and standard deviation (150 mm^3 in the first and 180 mm^3 in the second billet) confirm this conclusion. Another sign of the skewness: although 43%/49% of voids in the first/second billet are one-voxel voids, in both billets they form just 1% of the whole void volume. While the largest void in the first/second billet represent 6%/8% of the void volume; i.e., the volume of one void is 6/8 times of the sum of the volumes of thousands of voids. This feature of distribution might be important because, assuming that it is more likely that the large voids influence or even control the mechanical failure of material than do the small voids, this feature shows that there might be very few voids in each PSL specimen that can significantly affect the mechanical behavior of specimen. Some few voids can be much more influential than many other voids. In the process of generation of virtual voids, this feature of distribution must not at all be neglected.

To get a sense about the three-dimensional shape of voids, one can employ the mass moment of inertia which, for a continuous body rotating about a specified axis, is calculated by Eq. (4)

$$I_m = \int_V \rho(\rightarrow r) \rightarrow r^2 dV \tag{4}$$

Table 2. Statistical Data of the Void Principal Mass Moments of Inertia in Both Billets

Billet	MOI	Mean (mm^5)	Median (mm^5)	Standard deviation (mm^5)	Skewness	Kurtosis
First billet	I_{11}	300	0.10	15,000	75	6,100
	I_{22}	36,000	0.63	1,540,000	75	6,300
	I_{33}	36,300	0.63	1,550,000	75	6,300
Second billet	I_{11}	750	0.10	81,000	140	19,300
	I_{22}	43,000	0.63	2,270,000	110	13,500
	I_{33}	43,600	0.63	2,280,000	110	13,200

where $\rightarrow r$ is the radius vector to a point in the body from the specified axis through the origin, and $\rho(\rightarrow r)$ is the mass density at the tip of vector $\rightarrow r$. The integration is evaluated over the volume V of the body. Because the shape of voids is of interest, the mass density of voids was arbitrarily set to be 1.

All voids' principal mass moments of inertia have been calculated. By definition, if the moments of inertia about principal axes are not equal, the length of the principal axis corresponding to the larger moment of inertia is less than that of the principal axis corresponding to the smaller moment of inertia. The statistical study shows that the distributions of void principal mass moments of inertia are significantly skewed. Table 2 lists the statistical data of the principal moments of inertia. In this paper, I_{11} is the moment of inertia about the major principal axis of void; hence it is the smallest principal moment of inertia, while I_{33}, which is the moment of inertia about the minor principal axis, is obviously the largest one [Later in Fig. 8 it will be shown that usually (but not always) the void's major principal axis (Axis #1) lies along L direction, while its minor principal axis (Axis #3) lies along TT direction]. Considering the values stated in Table 2, one can conclude that the statistical properties of length, shape and location of voids are of the same order in the tested billets. Hence the void statistics is homogeneous all inside the parent PSL billet.

Aspect ratios of the principal moments of inertia can help to detect the shape of the voids. Fig. 7 displays how the aspect ratios are distributed.

Histograms shown in Fig. 7 illustrate clearly that in most of the voids, I_{11} is much smaller than two other almost equal principal moments of inertia, I_{22} and I_{33}. Therefore, in most voids, one of the principal axes is much larger than other two almost-equal axes. This conclusion is in agreement with the results taken from chord length density functions (Fig. 5).

Because the ultimate goal of this study is to virtually generate random voids and use them in the study of mechanics of PSL for making arbitrarily sized PSL models, the correlation coefficients of principal moments of inertia are as important as their distribution. Here are the matrices of correlation coefficients of principal moments of inertia for both billets

$$\rho_{I_{\text{first}}} = \begin{bmatrix} 1 & 0.96 & 0.96 \\ 0.96 & 1 & 1 \\ 0.96 & 1 & 1 \end{bmatrix} \tag{5}$$

$$\rho_{I_{\text{second}}} = \begin{bmatrix} 1 & 0.27 & 0.30 \\ 0.27 & 1 & 1 \\ 0.30 & 1 & 1 \end{bmatrix} \tag{6}$$

The major and second major moments of inertia (i.e., I_{33} and I_{22}) are perfectly correlated. This is because most of the voids grow just in the longitudinal direction and have the aspect ratio in the order of 1 in T-TT sections.

The probability density function of the coordinates of the void centroids is uniform over the billet domain in all material directions. The direction of voids, i.e., their angle with the material axes, is another piece of data required for void characterization. In the bottom-right corner of Fig. 8, the orientation of major principal axis of each void is depicted by a line with unit length. Fig. 8 presents the same data in stereographic form. Each point represents the projection of intersection of the lines shown in the figure at corner with a sphere with unit radius centered at the origin of T-TT plane. Obviously, almost all of the voids are aligned along the interval of $-30°$ to $30°$ of the longitudinal direction. A few voids, which are either very short or spherical, have made larger angles with the longitudinal direction. Therefore, it is reasonable to accept that all voids in the studied PSL billets are aligned in the longitudinal direction or make small angles with this direction. The principal angles were found to be uncorrelated.

Characterization through Equivalent Ellipsoids

To provide a methodology to generate virtual voids, it is reasonably favorable to approximate the actual shape of the voids with a known and defined shape. The observations and statistical data show that ellipsoidal shape might be a good approximation for actual void shape. This section is allocated to the verification of this hypothesis. Working with the ellipsoidal shapes instead of the actual arbitrary shapes eases the understanding of void characteristics and simulation of voids by finite element models.

Let a void be modeled by an ellipsoid with major axis half-length R_1 and minor axis half-lengths R_2 and R_3. The volume of such an ellipsoid is given by

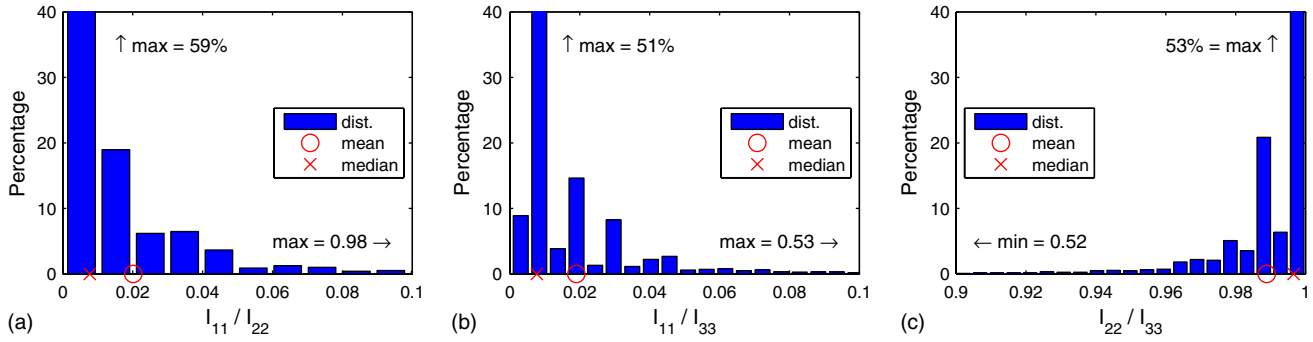

Fig. 7. Distribution of aspect ratio of principal moments of inertia of the first PSL billet voids: (a) minor/second major; (b) minor/major; (c) second major/major

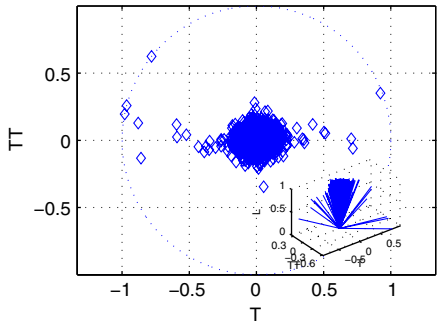

Fig. 8. Stereographic projection of the voids in the first billet with respect to longitudinal axis

$$V = \frac{4}{3}\pi R_1 R_2 R_3 \tag{7}$$

Based on the void geometry shown in Fig. 6 and Table 2, a reasonable initial assumption is that the ellipsoid's major radius R_1 is aligned with the void's major principal axis (based on Fig. 8, in most cases L direction), the second minor radius R_2 is aligned with the void's second minor principal axis (in most cases T direction), and the minor radius R_3 is aligned with the void's minor principal axis (in most cases TT direction). Assuming the unit density, the principal moments of inertia of ellipsoid are then

$$I_{11} = \frac{V(R_2^2 + R_3^2)}{5} \tag{8}$$

$$I_{22} = \frac{V(R_1^2 + R_3^2)}{5} \tag{9}$$

$$I_{33} = \frac{V(R_1^2 + R_2^2)}{5} \tag{10}$$

The goal of this model would be to calibrate the mean ellipsoid dimensions R_1, R_2, and R_3 to the statistics of section "Direct Characterization" and choose distributions of these parameters to match at least the second moment properties of the void mesostructure. It must be noted that setting Eqs. (7)–(10) equal to the mean values in Table 2 results in an over-determined system of equations that may not have an acceptable solution (four equations but three unknowns). An appropriate way to tackle this problem is to eliminate two unknowns (e.g., R_2 and R_3) by combining the equations and form two equations dependent on just one unknown (e.g., R_1). One can now minimize the square root of sum of the squares of these two equations and find the only remaining unknown. For example, by combining the Eqs. (7)–(10), it can be concluded

$$R_1^2 + \left[\frac{3V}{4\pi R_1\sqrt{\frac{5I_{33}}{V} - R_1^2}}\right]^2 + \frac{5I_{22}}{V} = 0 \tag{11}$$

$$\left(\frac{5I_{33}}{V} - R_1^2\right) + \left[\frac{3V}{4\pi R_1\sqrt{\frac{5I_{33}}{V} - R_1^2}}\right]^2 + \frac{5I_{11}}{V} = 0 \tag{12}$$

Note that V, I_{11}, I_{22} and I_{33} are the geometric properties of voids. R_1 is computable by minimizing SRSS of Eqs. 11 and 12. Once R_1 is calculated, R_2 and R_3 can be found using the following equations

$$R_2 = \sqrt{\frac{5I_{33}}{V} - R_1^2} \tag{13}$$

$$R_3 = \frac{3V}{4\pi R_1 R_2} \tag{14}$$

Fig. 9(a) illustrates a T-TT section of PSL where 2D voids have been replaced with equivalent ellipses. In Fig. 9(b), an equivalent ellipsoid has been fitted to a three-voxel void. To present the statistics of equivalent ellipsoids, Fig. 10 shows the distribution of radii of the equivalent ellipsoids. Also, histograms of aspect ratios of ellipsoids' moments of inertia are displayed in Fig. 11. According to this figure, the aspect ratios of moments of inertia of equivalent ellipsoids match well that of actual voids (Fig. 7). Table 3 compares the statistical measures of the moments of inertia of actual voids and their equivalent ellipsoids.

The matrices of correlation coefficients of equivalent ellipsoids' radii for the first and second billets are as follows:

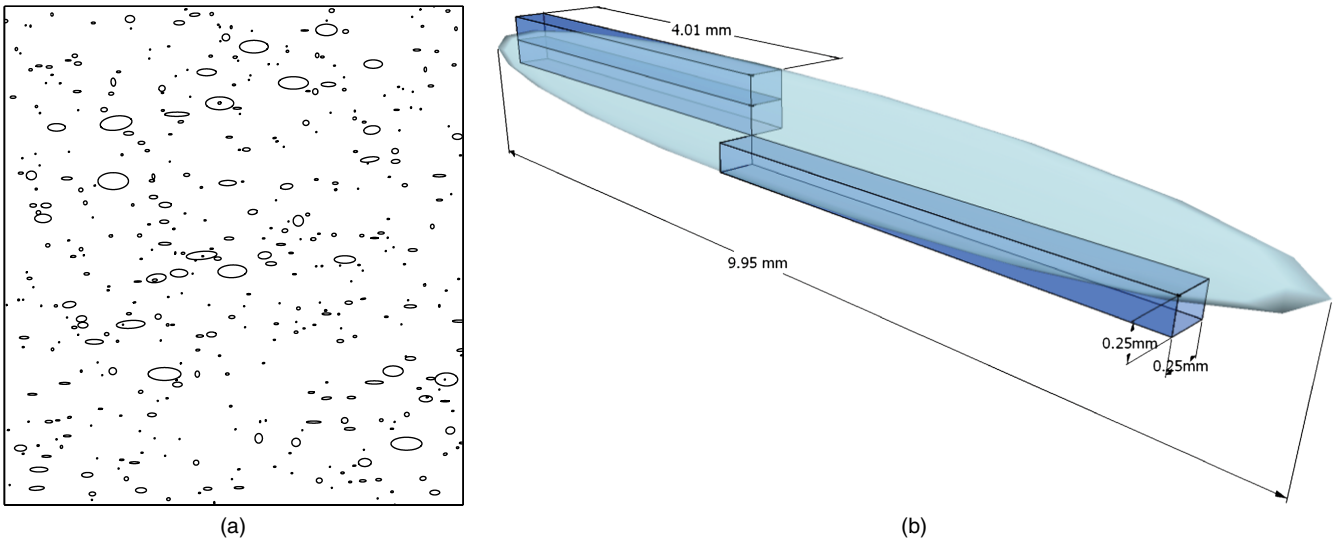

Fig. 9. 2D illustration of void replacements and a scheme of 3D replacement: (a) ellipses replaced 2D voids; (b) minor/major

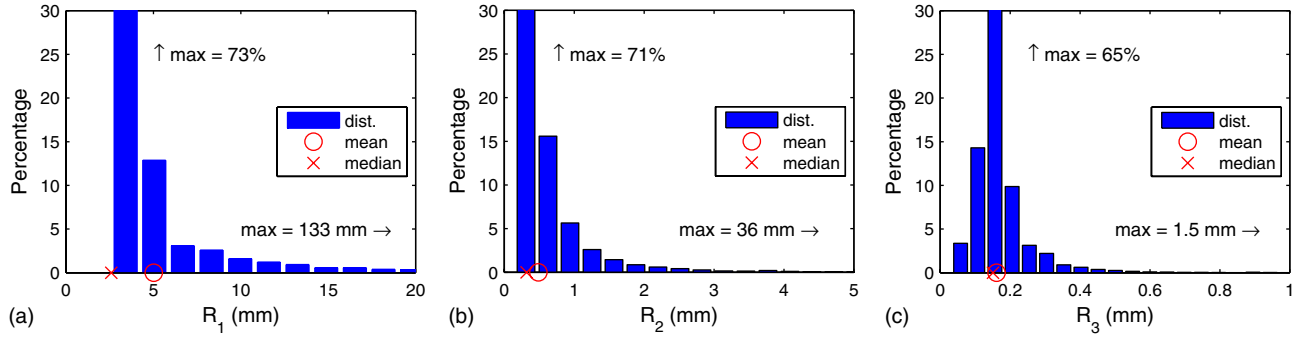

Fig. 10. Distribution of the radii of equivalent ellipsoids fitted to the voids of first billet: (a) major radius; (b) second minor radius; (c) minor radius

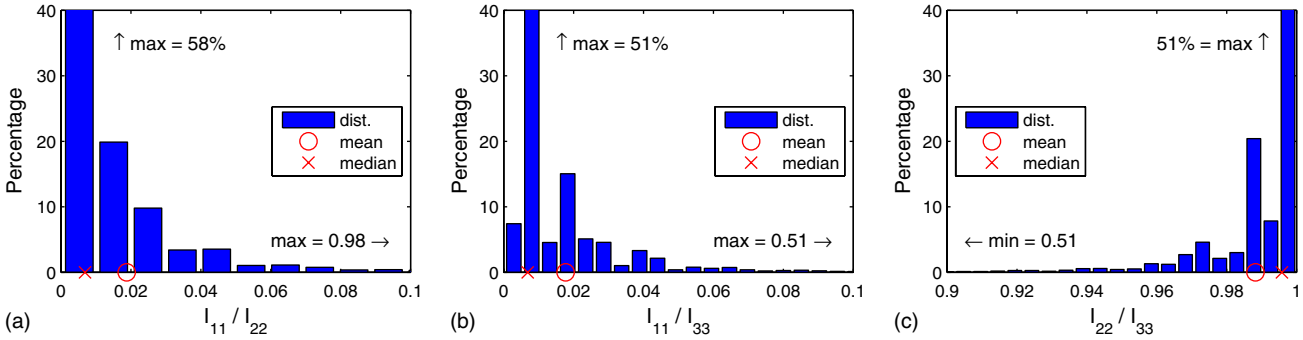

Fig. 11. Distribution of the aspect ratio of principal moments of inertia of equivalent ellipsoids fitted to the voids of first billet: (a) minor/second major; (b) minor/major; (c) second major/major

$$\rho_{R_{\text{first}}} = \begin{bmatrix} 1 & 0.81 & 0.28 \\ 0.81 & 1 & 0.34 \\ 0.28 & 0.34 & 1 \end{bmatrix} \tag{15}$$

$$\rho_{R_{\text{second}}} = \begin{bmatrix} 1 & 0.69 & 0.32 \\ 0.69 & 1 & 0.27 \\ 0.32 & 0.27 & 1 \end{bmatrix} \tag{16}$$

One should not expect to see a match between these correlation structures and the previous correlations introduced by Eqs. (5) and (6). Here, the correlation of radii with the dimension $[L]$ (length) are introduced, while the matrices 5 and 6 show the correlation of moments of inertia with the dimension $[L^5]$.

Probabilistic Model for PSL Mesostructure

Once the distributions of equivalent ellipsoids are obtained, one can generate virtual ellipsoidal voids with randomly generated radii, alignments and locations. Given that no clustering of voids was observed in the mesostructure, the centroids of the voids can be modeled by uniform distribution. But no mathematically known and defined distribution can be fitted to the distributions of ellipsoid radii (Fig. 10) and void principal angles. The translation model (Arwade 2005) was used to generate non-Gaussian random radii and angles with specified marginal target distributions and correlation functions [Eqs. (5) and (15)].

Suppose that the generation of a correlated non-Gaussian random vector, $\mathbf{Z} \in \mathbf{R^d}$, with components Z_i, mean m and covariance matrix $\mathbf{c}$ defined by $\mathbf{c} = \mathbf{E}[(\mathbf{Z} - \mu)(\mathbf{Z} - \mu)^T]$ is of interest [where $E(.)$ is the expectation operator]. According to the translation method, first a vector of uncorrelated Gaussian random variables, $\mathbf{Y} \in \mathbf{R^d}$ with components Y_i, is generated. Choleski decomposition this vector to a correlated Gaussian vector, $\mathbf{Y}'$ with components Y_i', using the target correlation coefficients (c_{ij}). This new correlated Gaussian vector can be transformed to a correlated non-Gaussian random vector, $\mathbf{Z}$, using the experimental cdf obtained from the target distributions. The transformation is given by

$$Z_i = F^{-1}[\Phi(Y_i')] \tag{17}$$

where $F(z)$ is the cumulative distribution function (cdf) of $\mathbf{Z}$ and $\Phi(.)$ is the standard (mean zero, unit variance) Gaussian cdf. In the case of this study, $\mathbf{Z}$ can be the vector of major (or any other type of) ellipsoid radii whose cumulative distribution function $[F(z)]$ has been evaluated empirically from the data of fitted equivalent ellipsoids.

Fig. 12 shows the distribution of the volume of virtually generated ellipsoidal voids that acceptably matches the distribution of the volume of actual voids in the first billet (Fig. 6). Therefore,

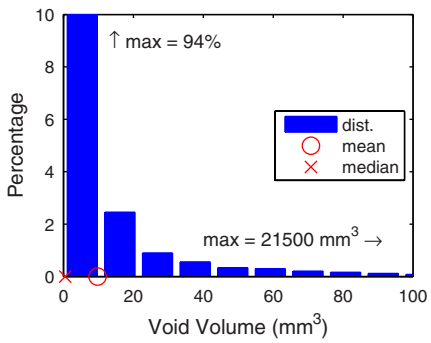

Fig. 12. Distribution of the volume of randomly generated virtual ellipsoids

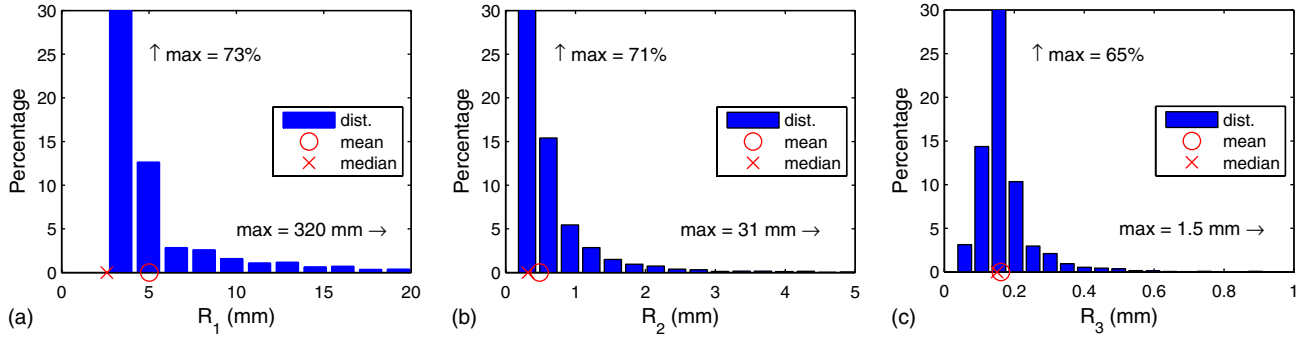

Fig. 13. Distribution of the radii of randomly generated virtual ellipsoids: (a) major radius; (b) second minor radius; (c) minor radius

Table 3. Comparison of the Statistics of the Voids of Both PSL Billets with Equivalent Ellipsoids

		Mean			Median		
Billet	Void type	I_{11} (mm^5)	I_{22} (mm^5)	I_{33} (mm^5)	I_{11} (mm^5)	I_{22} (mm^5)	I_{33} (mm^5)
First billet	Void	300	36,000	36,300	0.10	0.63	0.63
	Equivalent ellipsoid	275	36,000	36,300	0.10	0.63	0.63
Second billet	Void	750	43,000	43,600	0.10	0.63	0.63
	Equivalent ellipsoid	710	43,000	43,600	0.10	0.63	0.63

Table 4. Comparison of the Statistics of Actual and Virtual Voids

	Mean			Correlation		
Type	I_{11} (mm^5)	I_{22} (mm^5)	I_{33} (mm^5)	ρ_{12}	ρ_{13}	ρ_{23}
Actual	300	36,000	36,300	0.96	0.96	1.00
Virtual	300	44,800	45,100	0.92	0.92	1.00

one can generate virtual voids based on the statistical data provided in section "Direct Characterization" and virtually generate a PSL specimen with any arbitrary size.

Fig. 13 displays the distributions of radii of virtual ellipsoidal voids. They properly match the distributions of radii of equivalent ellipsoids shown in Fig. 10. It is also important that the correlation coefficients of virtual radii match the actual values; Eq. (18) shows a good agreement between correlation coefficients. Hence, the generation of virtual voids with the size and size correlation similar to actual ones is absolutely possible. More details about the comparison of the moments of inertia of actual and virtual voids are presented in Table 4.

$$\rho_R = \begin{bmatrix} 1 & 0.78 & 0.25 \\ 0.78 & 1 & 0.29 \\ 0.25 & 0.29 & 1 \end{bmatrix} \tag{18}$$

All in all, regarding the size, shape, location, and alignment of the voids, the randomly generated virtual ellipsoidal voids have the same 3D statistical data as the actual voids observed in the first PSL billet. This similarity was expected because the same distributions have been used in the process of ellipsoid generation.

The last step is to verify the validity of probabilistic model using 2D probability measures. A $51 \times 51 \times 152$ mm virtual PSL billet including randomly generated virtual ellipsoids was made. It is expected that the 2D probability functions used for characterization of actual voids return similar outputs for this virtual billet that has void volume fraction of 3.6%. Figs. 14 and 15 both show that the geometrical statistics of virtual ellipsoids are similar to that of the voids except for the fact that the average axis length of virtual ellipsoids in TT direction is more than that of actual voids. Also, unlike actual voids, the axis length of virtual ellipsoids in TT direction is on average larger than their axis length in T direction.

The reason for this bias is probably the bifurcation of voids. When actual voids have different branches lying along different directions, the method explained before to fit ellipsoids to actual voids does not work favorably and results in equivalent ellipsoids with unreasonable aspect ratio in T-TT plane. Since the radii of virtual ellipsoids are generated based on the distribution of radii of equivalent ellipsoids, virtual ellipsoids show the same bias. This bias does not influence the usefulness of virtual ellipsoids, because the average length of these ellipsoids in L direction (the major and most important direction) is still realistically much larger than that

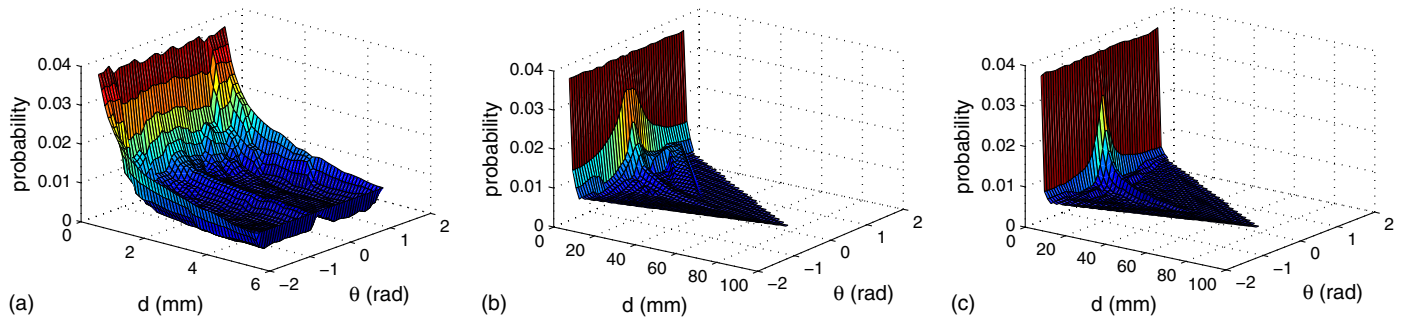

Fig. 14. Two-point probability functions for the virtual PSL billet: (a) T-TT section; (b) L-TT section; (c) L-T section

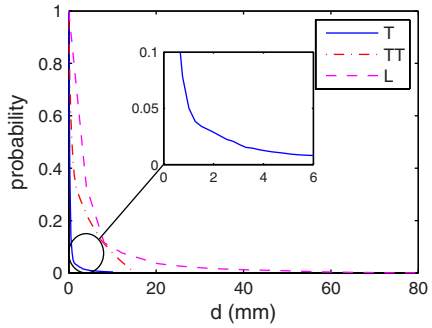

Fig. 15. Chord length density function in all three material directions of a virtually generated PSL billet

of the other two directions. In fact, one can assume that have been rotated with respect to their L axis. This rotation does not influence the mechanics of the PSL model along L direction. The mechanics of PSL along the other two directions will not be affected significantly either, because the lengths of ellipsoids in TT direction are still not large enough to change the material's mechanical behavior.

The probabilistic material model developed and validated here can have two primary applications: material design and the development of novel macroscopic constitutive models. In the first case, the existence of a probabilistic model for the void geometry allows material designers to investigate how changes in parameters describing the void geometry affect the void structure and eventually mechanical properties of the material. In the second case, the void model can be used to develop finite element models of PSL members, and simulation of the response of such models to various stress states can be used to develop or improve macroscopic constitutive models. In both cases, such numerical investigations would have to be supported and validated by experiments, but the presence of probabilistic numerical models holds the promise of accelerating the development of novel designs and constitutive models. Therefore, while it is not expected that a civil engineer would use a probabilistic void geometry model in the course of regular practice, models as presented here could lead to improved materials, and material models that would be of use in the usual practice of structural engineering.

Conclusion

To discover the nature of PSL heterogeneity, the mesostructure of material has been characterized via serial sectioning of two PSL billets, scanning the sections, developing computer programs to detect the voids, and conducting a statistical study on voids. Studies showed that most voids are elongated and aligned along the material longitudinal direction. On the other hand, the aspect ratios of void sections in T-TT planes are close to 1. An ellipsoid can be an appropriate replacement for such a void shape. The statistical study confirmed this inference. Variation in statistical properties of the void structure between the two tested billets is modest with regard to most characterizations although a more detailed study of void structure variability within billets and across batches is needed. Based on the output of the void characterization and statistics of equivalent ellipsoids, a probabilistic model has been introduced for the PSL mesostructure. The probabilistic material model developed and validated here can be applied in the material design and the development of novel macroscopic constitutive models.

References

Amini, A. (2013). "Mesostructural characterization and probabilistic modeling of the design limit states of parallel strand lumber." Ph.D. thesis, Univ. of Massachusetts, Amherst, MA.

Amini, A., Arwade, S. R., and Clouston, P. L. (2013). "Stochastic characteristics and modeling of structural composite lumber." *Proc., 11th Int. Conf. on Structural Safety and Reliability (ICOSSAR)*, Int. Association for Structural Safety and Reliability (IASSAR), New York, NY.

Arwade, S. R. (2005). "Translation vectors with non-identically distributed components." *Prob. Eng. Mech.*, 20(2), 158–167.

Arwade, S. R., Clouston, P. L., and Winans, R. (2009). "Measurement and stochastic computational modeling of the elastic properties of parallel strand lumber." *J. Eng. Mech.*, 10.1061/(ASCE)EM.1943-7889.0000020, 897–905.

Arwade, S. R., Winans, R., and Clouston, P. L. (2010). "Variability of the compressive strength of parallel strand lumber." *J. Eng. Mech.*, 10.1061/(ASCE)EM.1943-7889.0000079, 405–412.

Bejo, L., and Lang, E. M. (2004). "Simulation based modeling of the elastic properties of structural composite lumber." *Wood Fiber Sci.*, 36(3), 395–410.

Clouston, P. (2007). "Characterization and strength modeling of parallel-strand lumber." *Holzforschung*, 61(4), 394–399.

Clouston, P. L., and Lam, F. (2001). "Computational modeling of strand-based wood composites." *J. Eng. Mech.*, 10.1061/(ASCE)0733-9399(2001)127:8(844), 844–851.

Ellis, S., Dubois, J., and Avramidis, S. (1994). "Determination of parallam macroporosity by two optical techniques." *Wood Fiber Sci.*, 26(1), 70–77.

Mindess, S., Sukontasukkul, P., and Lam, F. (2004). "Fracture of air-dried and fully saturated parallel strand lumber (PSL) under impact loading." *Wood Sci. Technol.*, 38(3), 227–235.

Sugimori, M., and Lam, F. (1999). "Macro-void distribution analysis in strand-based wood composites using an X-ray computer tomography technique." *J. Wood Sci.*, 45(3), 254–257.

Torquato, S. (2002). *Random heterogeneous materials: Microstructure and macroscopic properties*, Vol. 16, Springer, New York.

U.S. Forest Products Laboratory (F. P. L). (2010). *Wood handbook: Wood as an engineering material*, Number 72. United States Government Printing.